pISSN 2384-1095
eISSN 2384-1109

iMRI 2020;24:123-131

https://doi.org/10.13104/imri.2020.24.3.123

iMRI
Investigative Magnetic Resonance Imaging

Optimization of Multi-Atlas Segmentation with Joint Label Fusion Algorithm for Automatic Segmentation in Prostate MR Imaging

Yoon Ho Choi[1], Jae-Hun Kim[2], Chan Kyo Kim[2,3,4]

[1]Department of Health Sciences and Technology, SAIHST, Sungkyunkwan University, Seoul, Korea
[2]Department of Radiology and Center for Imaging Science, Samsung Medical Center, Sungkyunkwan University School of Medicine, Seoul, Korea
[3]Department of Medical Device Management and Research, SAIHST, Sungkyunkwan University, Seoul, Korea
[4]Department of Digital Health, SAIHST, Sungkyunkwan University, Seoul, Korea

Original Article

Received: April 2, 2020
Revised: May 14, 2020
Accepted: July 18, 2020

These authors (C.K.K. and J.K.) contributed equally to this study.

Correspondence to:
Chan Kyo Kim, M.D., Ph.D.
Department of Radiology, Samsung Medical Center, Sungkyunkwan University School of Medicine, 81 Irwon-ro, Gangnam-gu, Seoul 06351, Korea.
Tel. +82-2-3410-0511
Fax. +82-2-3410-2559
E-mail: chankyokim@skku.edu

Purpose: Joint label fusion (JLF) is a popular multi-atlas-based segmentation algorithm, which compensates for dependent errors that may exist between atlases. However, in order to get good segmentation results, it is very important to set the several free parameters of the algorithm to optimal values. In this study, we first investigate the feasibility of a JLF algorithm for prostate segmentation in MR images, and then suggest the optimal set of parameters for the automatic prostate segmentation by validating the results of each parameter combination.

Materials and Methods: We acquired T2-weighted prostate MR images from 20 normal heathy volunteers and did a series of cross validations for every set of parameters of JLF. In each case, the atlases were rigidly registered for the target image. Then, we calculated their voting weights for label fusion from each combination of JLF's parameters (r_{pxy}, r_{pz}, r_{sxy}, r_{sz}, β). We evaluated the segmentation performances by five validation metrics of the Prostate MR Image Segmentation challenge.

Results: As the number of voxels participating in the voting weight calculation and the number of referenced atlases is increased, the overall segmentation performance is gradually improved. The JLF algorithm showed the best results for dice similarity coefficient, 0.8495 $\pm$ 0.0392; relative volume difference, 15.2353 $\pm$ 17.2350; absolute relative volume difference, 18.8710 $\pm$ 13.1546; 95% Hausdorff distance, 7.2366 $\pm$ 1.8502; and average boundary distance, 2.2107 $\pm$ 0.4972; in parameters of $r_{pxy} = 10$, $r_{pz} = 1$, $r_{sxy} = 3$, $r_{sz} = 1$, and $\beta = 3$.

Conclusion: The evaluated results showed the feasibility of the JLF algorithm for automatic segmentation of prostate MRI. This empirical analysis of segmentation results by label fusion allows for the appropriate setting of parameters.

Keywords: Prostate; Magnetic resonance imaging; Multi-atlas based segmentation; Joint label fusion; Automatic prostate segmentation

INTRODUCTION

Prostate cancer is a worldwide major health concern. According to the American Cancer Society in 2019, prostate cancer will record the highest incidence (20%) and the second-highest death rate (10%) among all cancer sites in American men (1). Generally, diverse medical imaging modalities, such as computed tomography (CT), magnetic resonance imaging (MRI) and trans-rectal ultrasound, are used for the diagnosis and treatment of prostate cancer, because they can provide intuitive anatomical information in a non-invasive manner. Of them, MRI is most commonly used because of its better soft-tissue contrast and higher sensitivity for detecting prostate cancer (2-5).

Segmentation of the prostate in an MR image is a primary essential step in clinical applications, such as radiotherapy planning, biopsy, and computer-aided diagnosis system (6). The delineated prostate area is directly used in the subsequent processes, such as boundary localization, volume estimation, or multimodal registration of the prostate area, which requires accurate and robust segmentation results.

In segmenting prostate regions from MR images, there are some challenges. Usually, since the prostate MR image has thick slices, it is difficult to distinguish the exact prostate area that exhibits various changes in appearance among the MR image slices. In addition, each patient has different sizes and shapes of the prostate, and the internal structure of the prostate is complicated. Furthermore, although the manual segmentation approach of the radiologist is available to delineate the prostate area of the MR image by slice, it is time consuming, is prone to error, and shows inter- and intra-observer differences caused by perspective differences.

To address these challenging tasks in manual prostate segmentation, many automatic or semi-automatic segmentation approaches have been suggested, ranging from low-level schemes that involve little prior information to high-level schemes that highly rely on prior knowledge (7-9). Among them, the principles of multi-atlas-based segmentation have been successfully applied to segmentation of the prostate area in MR images (10-12). In contrast to other low-level segmentation approaches, such as edge-based or deformable-model-based segmentation, this high-level approach has a major advantage in introducing *a priori* knowledge about the distribution of the internal structure of the target (8). This property leads to the effective segmentation of the prostate area, which has a complex internal structure, such as a central zone and a peripheral zone under the different sizes, shapes, and intensity distribution of the prostate for each patient.

In this study, we implemented the multi-atlas segmentation with the joint label fusion (MAS-JLF) algorithm and examined the optimal parameters for automatic segmentation of the prostate in T2-weighted MRI. We used twenty T2-wegihted MR images from our hospital for our experiments and evaluated the performance of the proposed algorithm by measurements used in the PROMISE12 challenge, a prostate segmentation challenge of the 2012 Medical Image Computing and Computer Assisted Interventions Conference (MICCAI12) (13) .

MATERIALS AND METHODS

Multi-Atlas-Based Label Fusion

In the multi-atlas segmentation procedure, a target image F_T is segmented by referencing a set of n registered atlases

$$A_1 = (F_1, S_1), \ldots, A_n = (F_n, S_n).$$

Here, the ith atlas A_i consisted of a set of (F_i, S_i) which denotes the registered atlas image of the target image and its corresponding segmented target region, or label image, respectively. Each registered atlas is considered to be one candidate segmentation of the target and as containing some segmentation/registration errors. Under the assumption that the label errors caused by registration and segmentation are independent, the label fusion process, integrating the atlases, produces better segmentation of the target image. Since most of the label fusion methods, however, deliberate removing independent errors in each atlas, the dependent label errors induced by different atlases may be correlated still remain. Therefore, the JLF was proposed to reduce the dependent label errors.

Joint Label Fusion

The JLF algorithm suggests including a dependency matrix of the pairwise atlases when computing weights in the label fusion process (14). By searching the minimum total expected error between true segmentation $S_T(x)$ and the consensus segmented result for the target label image $\bar{S}(x)$, adequate weights are distributed to each atlas.

In order to find the minimum total expected error, first of all, the JLF algorithm models segmentation error in binary representation as:

$$S_T(x) = S_i(x) + \delta^i(x), \quad [1]$$

where $\delta^i(x)$ indicates the label difference between the ith atlas label image ($S_T(x)$) and the target true segmentation ($S_T(x)$) at the same position x. Since the label error occurs when the value of the label difference is -1 or 1, the label difference can be described as a discrete random variable, characterized by the following distribution:

$$q^i(x) = p(|\delta^i(x)| = 1 | F_T, F_1, \ldots, F_n). \quad [2]$$

The JLF algorithm applies a weighted voting scheme that assigns non-negative local weights to each atlas to estimate the consensus segmentation, which in weighted voting is obtained by

$$\bar{S}_T(x) = \sum_{i=1}^{n} w_i(x) S_i(x) \quad [3]$$

and the sum of weights is 1 in Eq [3].

With Eqs. [1] and [3], the total expected error can be found as follows:

$$E_{\delta^1(x), \ldots, \delta^n(x)} [(S_T(x) - \bar{S}(x)) \mid F_T, F_1, \ldots, F_n]$$

$$= E_{\delta^1(x), \ldots, \delta^n(x)} \left[\left(\sum_{i=1}^{n} w_i(x) \delta^i(x) \right)^2 \mid F_T, F_1, \ldots, F_n \right] \quad [4]$$

$$= \sum_{i=1}^{n} \sum_{j=1}^{n} w_i(x) w_j(x) E_{\delta^1(x), \delta^j(x)} [\delta^i(x) \delta^j(x) | F_T, F_1, \ldots, F_n]$$

$$= W_x^t M_x W_x,$$

where W_x is the set of voting weights $[W_1(x); \ldots; W_n(x)]$, t represents transpose, and $M_x(i,j)$, called a pairwise dependency matrix from atlas i and j, is estimated from intensity dis-similarity between each pair of atlas images i and j.

$$M_x(i,j) = p(\delta^i(x)\, \delta^j(x) = 1 | \{F_T(y), F_i(y), F_j(y) | y \in N(x)\})$$
$$\propto [\textstyle\sum_{y \in N(x)} |F_T(y) - F_i(y)| |F_T(y) - F_j(y)|]^{\beta}, \quad [5]$$

where N(x) indicates a cubical neighborhood around x, the size of the local appearance patch is determined by patch radius r, and β indicates the controlling parameter for weight distribution to estimate M_x. By applying Lagrange multipliers with the pre-determined dependency matrix M_x, the optimal weight set W_x that minimizes the total expected error can be found.

Registration Error Refinement in JLF

In the JLF algorithm, registration errors can be regulated by finding neighborhood point x' around x that produces a better local intensity similarity patch $F_i[N(x')]$ against the original local patch $F_i[N(x)]$ in the same ith registered atlas image. As for finding the point x' that makes the local patch $F_i[N(x')]$ most similar to the target local patch $F_T[N(x)]$, radius r_s of a cubical local search patch $N_s(x)$ is applied.

The local search correspondence map between the ith atlas and the target images can be described as follows:

$$\varepsilon_i(x) = \arg\min_{x' \in N_s(x)} ||F_i(N(x')) - F_T(N(x))||^2 \quad [6]$$

Once the set of maps $\{\varepsilon_i\}$ is filled, the definition of the consensus segmentation, Eq. [3], is refined as

$$\bar{S}_T(x) = \sum_{i=1}^{n} w_i(\varepsilon_i(x)) S_i(\varepsilon_i(x)) \quad [7]$$

Experiments and Evaluation

Twenty healthy volunteers underwent T2-weighted imaging under the approval of the local Institutional Review Board. We obtained all MRI data with a 3T clinical MR scanner (Achieva TX, Philips Healthcare, Best, the Netherlands) with a phased-arrayed coil. The parameters were as follows: repetition time/echo time, 3459/100 msec; slice thickness, 3 mm; interslice gap, 1 mm; matrix, 568 × 341 matrix; field of view, 20 cm and in-plane resolution, 0.35 × 0.59 × 4 mm^3. For each subject, the whole prostate area was manually defined by an experienced radiologist and used as the standard of reference. We evaluated the segmentation performance for each combination of JLF algorithm parameters by doing a leave-one-out test. At first, we set one of the 20 atlases as the target image, and randomly selected the reference images from the remaining 19 atlases (10, 15, and 19 reference images). Then, prior to the execution of the label fusion algorithm, we did the registration of multiple atlases for the target image. In this process, we used FMRIB's Software Library (FSL, http://www.fmrib.ox.ac.uk/fsl) (15) for rigid body registration in 7 degrees of freedom. Next, we did whole prostate segmentations for the target image with each set of input parameters of all possible combinations of JLF. In this way, we iteratively conducted the JLF to find the optimal parameters from combinations within the free parameters until all the atlas were set to the target image once. For

optimal parameter searching, we investigated different patch-radius parameters for the xy plane and z axis, unlike the patch parameters of the original JLF algorithm with the same radius for the x, y, and z axes. Since the original JLF algorithm assumed that all participating images were made by using isovoxels, all patches were cubical. However, because our images are anisotropic, with slice thicknesses much longer than in-plane resolution, it is not appropriate to set the z-axis radius of each patch equal to the xy-plane radius. Therefore the parameters in our study are as follows:

- r_{p_xy}, the radius in the xy-plane of the local appearance patch N used for the similarity-based dependency matrix M_x estimation;
- r_{p_z}, the radius in the z axis of the local appearance patch;
- r_{s_xy}, the radius in the xy plane of the local searching patch N_s that is used in refining registration errors;
- r_{s_z}, the radius in the z axis of the local searching patch; and
- β, the parameter used to transfer image similarities in the pairwise joint label difference term.

The range of each parameter was as follows:

- $r_{p\_xy} \in \{3, 4, 5, 6, 7, 8, 9, 10\}$,
- $r_{p\_z} \in \{0, 1\}$,
- $r_{s\_xy} \in \{0, 1, 2, 3\}$,
- $r_{s\_z} \in \{0, 1\}$, and
- $\beta \in \{1, 2, 3, 4, 5, 6, 7, 8\}$.

The unit of radius for a patch is a voxel in our experiments. Thereafter, we evaluated the 20480 prostate segmentation results by each combination of parameters and the atlas set by the four metrics described in the Evaluation Method section. We used the implemented JLF software imported from Github's ANT repository (https://github.com /stnava/ANTs/blob/master/Scripts/antsJointLabelFusion.sh) and executed it on an Intel®Core ™ i7-6850K CPU @ 3.60 GHz × 12, and 62 GB memory environment.

Evaluation Method

The PROMISE12 challenge was held to allow a fair comparison of segmentation methods based on performance and robustness (11). In the challenge, each result of a proposed segmentation algorithm was evaluated using volume and boundary measurements to give more a complete perspective of segmentation accuracy. In our study, we used the metrics of dice similarity coefficient (DSC), relative volume difference (RVD), average boundary distance (ABD), absolute relative volume difference (aRVD), and 95% Hausdorff distance (HD) to evaluate the prostate segmentation results produced by JLF for the various parameters.

The DSC can be acquired by

$$D(X,Y) = \frac{2|X \cap Y|}{|X| + |Y|}, \quad [8]$$

where $|X|$ denotes the number of voxels in the reference region and $|Y|$ indicates the number of voxels in the algorithm produced region. The RVD was calculated using:

$$RVD(X,Y) = 100\times\left(\frac{|X|}{|Y|} - 1\right). \quad [9]$$

Therefore, the aRVD is

$$aRVD(X,Y) = |RVD(X,Y)|. \quad [10]$$

In fact, PROMISE 12 used RVD to measure only the average tendency of whether the algorithm is over- or under-segmentation. In this work, we also measured aRVD by, Eq. [10].

The regular HD is calculated as:

$$HD_{asym}(X_s,Y_s) = \max_{x\in X_s} \min_{y\in Y_s} d(x,y) \quad [11]$$

$$HD(X_s, Y_s) = \max(HD_{asym}(X_s, Y_s), HD_{asym}(Y_s, X_s)), \quad [12]$$

where X_s indicates the set of surface points of the reference region and Y_s is that of algorithm-produced regions. The Euclidean distance operator is indicated as d. Since the regular Hausdorff distance is too sensitive to trust, the PROMISE12 challenge adopted the 95th percentile of the asymmetric 95% HD in place of the maximum. as we did also.

At last, the ABD is described as:

$$ABD(X_s, Y_s) = \frac{1}{N_{Xs}+N_{Ys}}\left(\sum_{x\in Xs}\min_{y\in Ys} d(x,y) + \sum_{y\in Ys}\min_{x\in Xs} d(y,x)\right). \quad [12]$$

We computed all the metrics employed in this study in three dimensions and applied them to not only the entire prostate region but also the apex and base parts of the prostate. In the slice dimension, we considered the cranial and caudal third of the prostate volume as the base and apex, respectively.

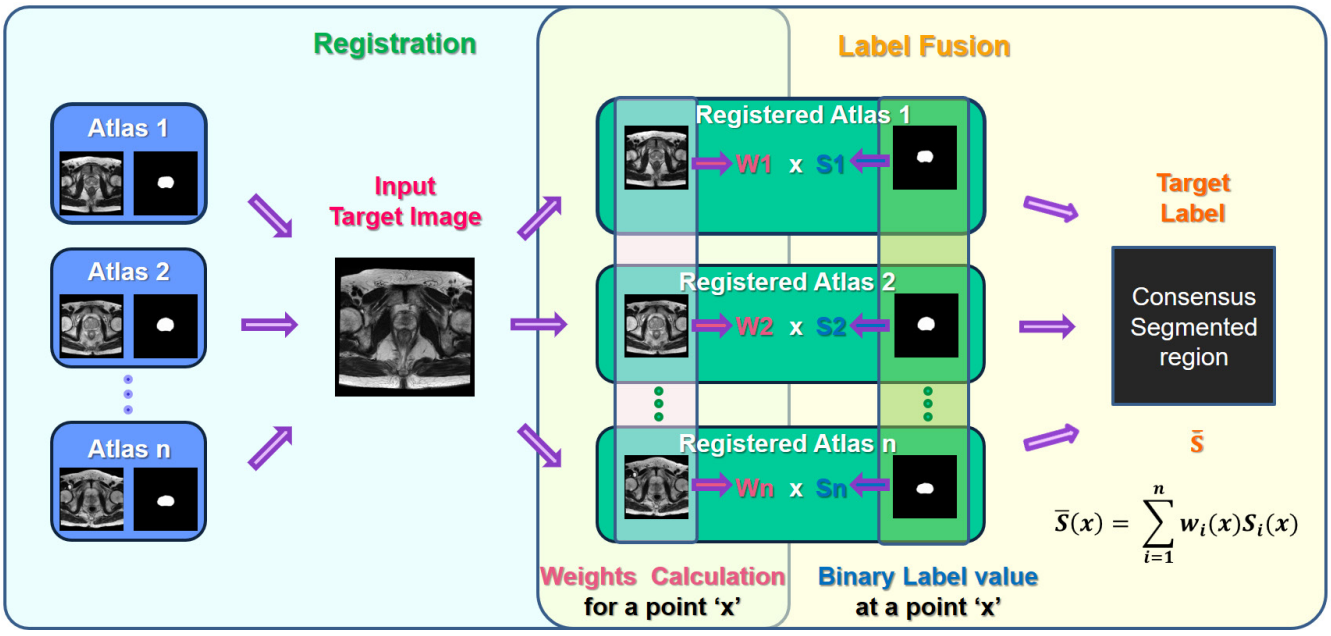

Fig. 1. Overview of the general workflow of the multi-atlas segmentation.

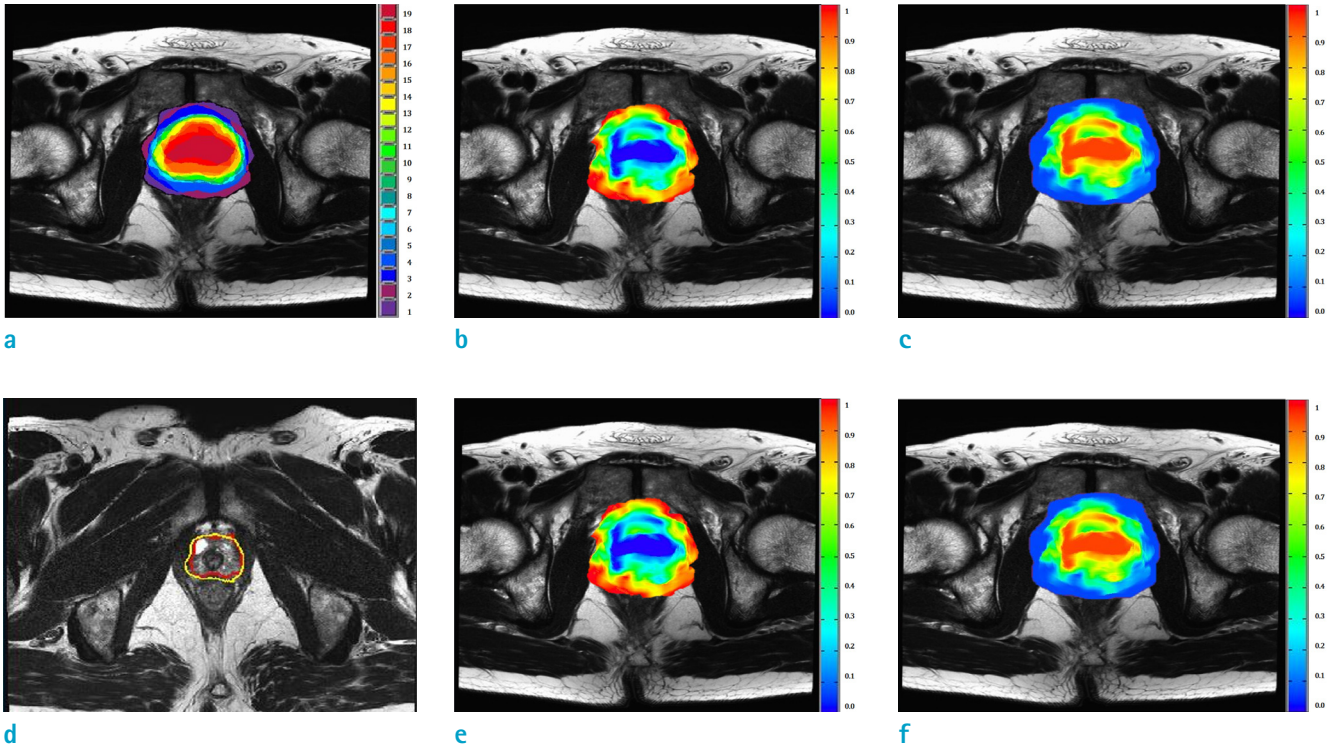

Fig. 2. Prostate segmentation processing with JLF for a representative subject. The voxels in the overlapping region of rigid-body registered atlas MR images into a target MR image (a) are considered as prostate candidates. From the candidates, posterior probability maps of voxels for non-prostate (b) and prostate (c) are developed and used to find the final segmentation. Final segmentation results are seen at the apex (d), midgland (e) and base (f) of the prostate. Red, gold standard. Yellow, automatically segmented prostate region.

RESULTS

MAS-JLF for Automatic Segmentation of the Prostate in MRI

Figure 1 shows the flowchart of the MAS with JLF for the automatic segmentation of the prostate in T2-weighted MRI. The multi-atlas was spatially transformed into a target image, and then the registered multi-atlas and labels were jointly fused to produce the posterior probability map for segmentation of the prostate. Figure 2 shows the representative results using the MAS-JLF algorithm for the segmentation of the prostate in T2-weighted MRI.

Optimization of the Patch Radius

In the MAS-JLF algorithm, the registered multi-atlas was fused to make a final result using the local similarity (dissimilarity) between the multi-atlases. The local similarity was computed depending on the patch radius, which determined how many voxels were included to compute the similarity between the multi-atlases. We examined the performance of the MAS-JLF according to the various patch radii. Figure 3 shows the results of the segmentation performance evaluation according to the z-axis radius of each patch (r_{p_z}, r_{s_z}) and the xy-plane radius of the appearance patch (r_{p_xy}). In our work, the parameters r_{s_xy} and β are set to 3. Both patches showed the best segmentation performance when the z-axis radius was 1, and the best xy-plane radius of the appearance patch was 10 (r_{p_z}=1, r_{s_z}=1, and r_{p_xy}=10). This result is close to the common-sense notion that local similarity computations and registration error corrections based on wider spatial information yield better performance.

Optimization of the Search Radius

The mis -registration of the multi-atlas into the target image could be lead to a poor performance of the MAS-JLF algorithm. To compensate for the error of the registration, we defined the search radius in the MAS-JLF algorithm. Figure 4 compares the segmentation performance of the parameter combinations of the search patch's xy-plane radius r_{s_xy} and the weight distribution controlling parameter β. The xy-plane radius and z-axis radius of the local appearance patch (r_{p_z}, r_{p_xy}), and the z-axis radius of the search patch (r_{s_z}) are set to the best values described right above, aRVD. When the parameter r_{s_xy} was set to 3, the segmentation results were the best for all metrics. Also, JLF showed the best segmentation performance when β was 3. The volume of the prostate region-of-interest obtained

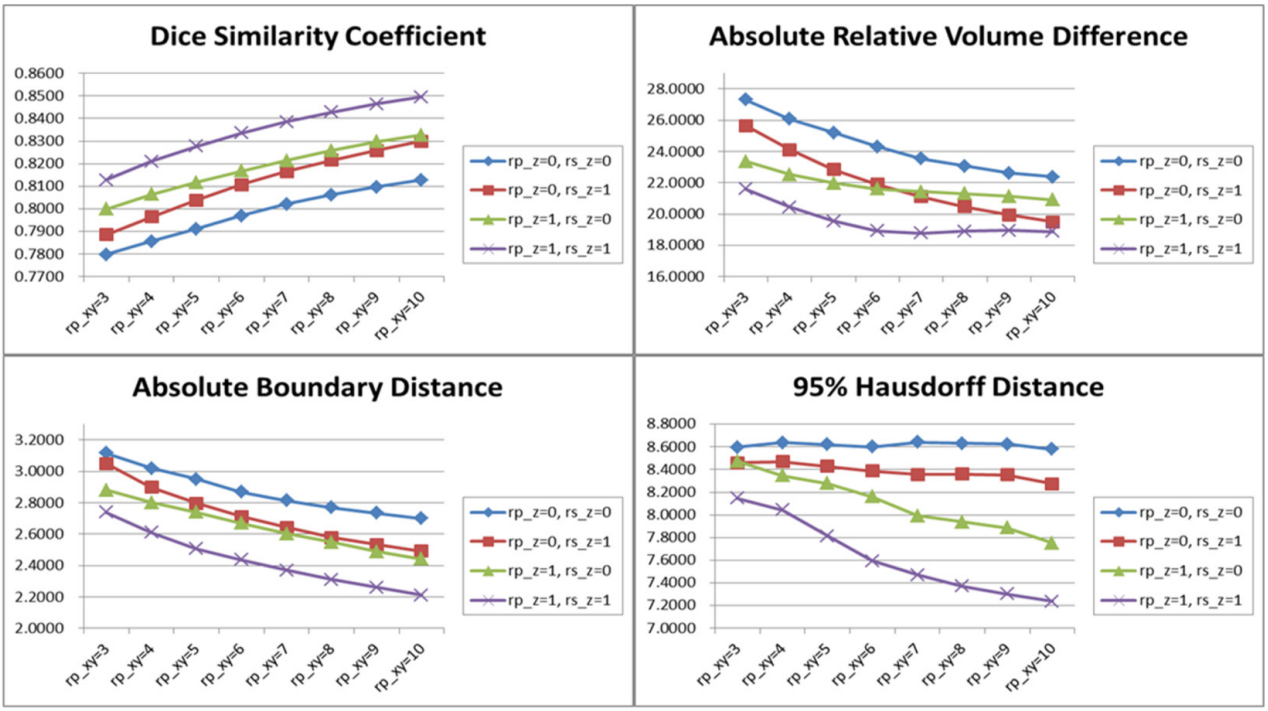

Fig. 3. Evaluation of prostate segmentation performance for the parameters r_{p_xy}, r_{p_z}, r_{s_z} of JLF algorithm by metrics of DSC, aRVD, ABD and 95% HD. Here the r_{s_xy}, and β are set to 3.

from a manual approach and automatic segmentation by JLF with the optimal parameters (r_{p_xy}= 10, r_{p_z}= 1, r_{s_xy}= 3, r_{s_z}= 1, and β = 3) was 40328 ± 11463 and 44628 ± 5923 mm^3, respectively (P > 0.05). The DSC of the segmentation results for the parameters was 0.8495 ± 0.0392, RVD was 15.2353 ± 17.2350, aRVD was 18.8710 ± 13.1546, 95% HD was 7.2366 ± 1.8502, and ABD was 2.2107 ± 0.4972. Table 1 shows the segmentation performance validation results for the prostate sub-regions consisting of base, midgland, and apex with DSC, RVD, aRVD, 95% HD, and ABD metrics from the best parameters of JLF. The mean time of the JLF algorithm for optimal parameters was 109 min 6 sec.

Optimization of the Number of Multi-Atlases

We examined the performance of the MAS-JLF algorithm according to the number of multi-atlases. Figure 5 presents

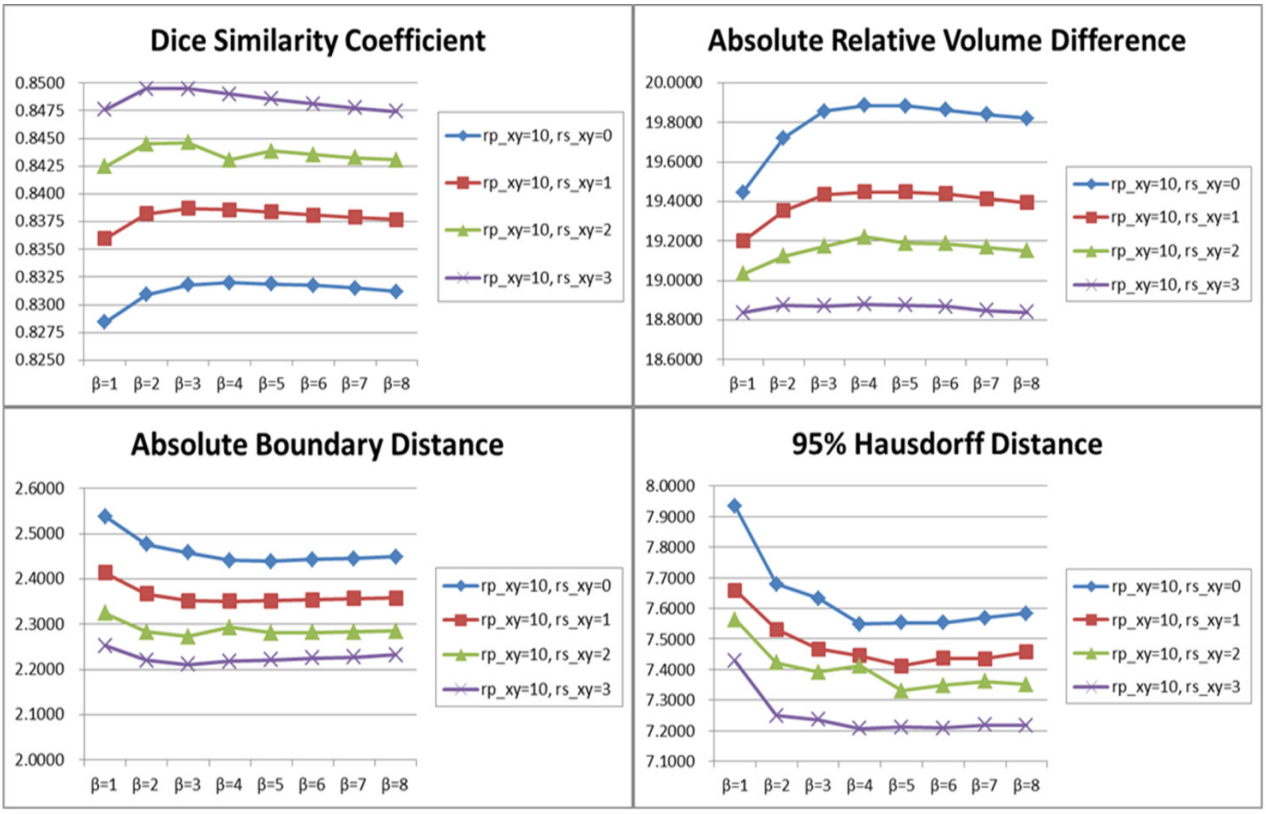

Fig. 4. Evaluation of prostate segmentation performance for the parameters r_{s_xy}, and β of JLF algorithm by metrics of DSC, ABD and 95% HD. Here the r_{p_xy}, r_{p_z}, r_{s_z} are set to 10, 1, and 1, respectively.

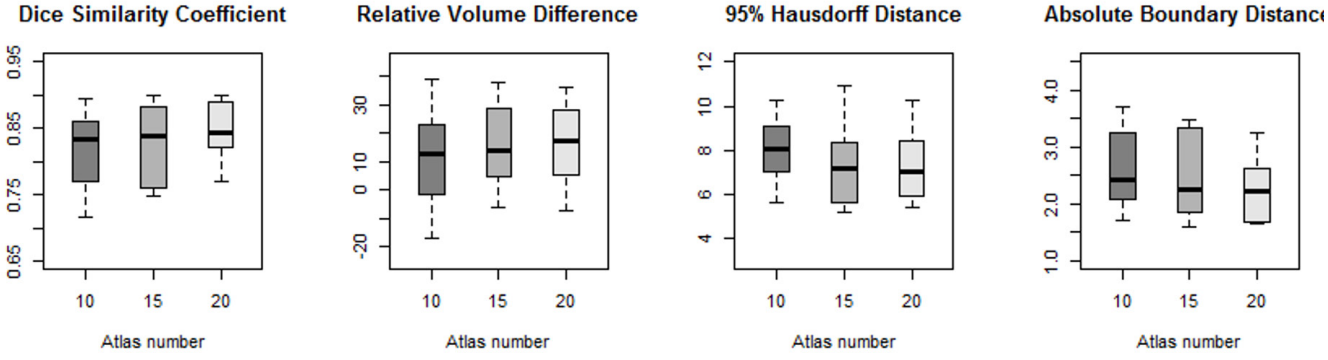

Fig. 5. Comparisons of segmentation performance evaluation according to the number of referenced atlases. The JLF algorithm is set to the best parameters: r_{p_xy}= 10, r_{p_z}= 1, r_{s_xy}= 3, r_{s_z}= 1, and β = 3.

Table 1. Prostate Segmentation Performance Evaluation for the Best Parameters: r_{pxy}= 10, r_{pz}= 1, r_{s_xy}= 3, r_{sz}= 1, and β = 3

Variable	Overall	Base	Midgland	Apex
Dice similarity coefficient	0.84595 ± 0.0392	0.8187 ± 0.0479	0.9055 ± 0.0434	0.7463 ± 0.1391
Relative volume difference	15.2353 ± 17.2350	8.2183 ± 25.3651	8.1217 ± 14.2708	70.5312 ± 89.3609
Absolute relative volume difference	18.8710 ± 13.1546	19.8726 ± 17.7766	10.6937 ± 12.4605	70.6291 ± 89.2835
95% Hausdorff distance	7.2366 ± 1.8502	7.0904 ± 1.5296	25.2330 ± 2.0698	7.2721 ± 2.7053
Average boundary distance	2.2107 ± 0.4972	2.4385 ± 0.5223	1.7169 ± 0.7466	2.7907 ± 1.2635

the results for the 10, 15, and 20 atlases, which confirm the principle of MAS that results are more stable and accurate as the number of referenced atlases increases. However, the average time cost according to the number of referenced atlases was 45 min 12 sec for 10, 80 min 12 sec for 15, and 109 min 6 sec for 20. Therefore, the number of atlases appropriate for the application environment should be selected in practice.

DISCUSSION

In a multi-atlas-based segmentation algorithm using weights by local similarity, the segmentation performance is seriously influenced by the number of referenced atlases and the size of the local appearance patch effects. The more atlases are used, the more stable and better segmentation is possible, but the computational complexity also increases. This makes it difficult to apply the MAS approach to segmentation tasks in addition to registration, which must be done as preprocessing. Therefore, it is definitely necessary to investigate the parameter settings and number of atlases that are relatively stable, perform well, and consume the least time

The computational complexity of the JLF algorithm is proportional to the size of the local appearance patch and of the search patch. Thus, we did experiments to find the optimum patch shape with better performance when referring to a similar number of voxels.

In the original JLF study (14), the local shape patch had the same size radius for all three (x, y, and z) axes to calculate the local similarity between the atlas and the target from the cubical region. However, they segmented brain hippocampal T1-weighted MR images with 1.0×1.0×1.0 mm^3 voxel resolution and 176 slice dimensions. Since our dataset has 21 slice dimensions in 0.35 × 0.59 × 4 mm^3 voxel resolution, setting the local appearance patch to have the same radius on the x, y, and z axes could not refer to the cubical region. Therefore, when applying JLF to non-isovoxel images, it is more effective to set a cuboid patch that references more voxels of a high-resolution plane than a cubical patch does.

Actually, the major factor that increases the computational complexity of JLF is the size of the search patch needed to correct the registration errors. The search patch may have a different shape and radius depending on the performance of the registration. However, we assume that the optimal shape of the search patch is related to the voxel resolution in the image, because the registration algorithm is based on the appearance of the image. In our study, we did an additional experiment to examine the performance of the MAS-JLF algorithm according to search radius of 0×0×0, 1×1×1, 2×2×2, and 3×3×3 when β was fixed at 3 (Supplementary Fig. 1). From these additional experiments, we can get a better result if the radius is 1 or 2. Given these experimental results, we set the range of the z-axis radius of the search patch and local appearance patch in this study to {0,1}.

In optimal parameters selection, unlike other parameters, which have a common tendency for all measurement metrics, it was hard to find the best value for β, because of the ambiguity of the measurement results. In PROMISE12, the values from the four metrics were aggregated and then the segmentation results of the algorithm were scored. But the scoring method was not available for us, because it requires having manual segmentation results from a second observer with a career of about two years besides the ground truth from an expert. So we concluded thar the qualitatively best parameter value of β as 3, which showed stabler and better performance for the other values in the four metrics.

For the segmentation performance evaluation of the sub-regions, the criteria for dividing the prostate from the image into base, center, and apex followed those of PROMISE12 (13). The base and apex of the prostate are the most difficult areas to segment and are a challenging task for all prostate segmentation algorithms. In Table 1, JLF also

worked less well for the base and apex than in the center, like other proposed segmentation algorithms. Especially, the apex region showed higher RVD and aRVD values than did the other two regions' we think that the under-segmentation tendency of JLF is mainly due to the apex.

CONCLUSION

In this paper, we segment the whole prostate using a multi-atlas-based JLF algorithm in T2-weghted MR images and investigate the feasibility of the JLF algorithm for the prostate segmentation by finding the optimal parameters. To segment the prostate, we modified the parameters of the JLF algorithm appropriately to fit our work and evaluated the segmentation performance in each parameter set by five evaluation metrics that are widely used. In our study, the result using the JLF algorithm is the best for DSC, 0.8495 ± 0.0392; RVD,15.2353 ± 17.2350; aRVD, 18.8710 ± 13.1546; 95% HD, 7.2366 ± 1.8502; and ABD, 2.2107 ± 0.4972, using parameters of r_{p_xy}= 10, r_{p_z}= 1, r_{s_xy}= 3, r_{s_z}= 1, and β = 3. This suggests the feasibility of the JLF method for automatic segmentation of prostate MR images. Finding the optimized parameters for segmenting a particular organ is important for practical clinical applications. Accordingly, at the end, we hope that the results of this study carefully pave the way for the prostate segmentation studies using MAS.

Supplementary Materials

The Data Supplement is available with this article at https://doi.org/10.13104/imri.2020.24.3.123

Acknowledgements

This work was supported by the genitourinary MRI study group of the Korean Society of Magnetic Resonance in Medicine (KSMRM) and the Basic Science Research Program through the National Research Foundation of Korea (NRF) funded by the Ministry of Education (NRF-2017R1A2B4006020).

REFERENCES

1. Siegel RL, Miller KD, Jemal A. Cancer Statistics, 2017. CA Cancer J Clin 2017;67:7-30
2. Rosenkrantz AB, Oto A, Turkbey B, Westphalen AC. Prostate Imaging Reporting and Data System (PI-RADS), version 2: a critical look. AJR Am J Roentgenol 2016;206:1179-1183
3. Weinreb JC, Barentsz JO, Choyke PL, et al. PI-RADS Prostate Imaging - Reporting and Data System: 2015, version 2. Eur Urol 2016;69:16-40
4. Yoon JM, Choi MH, Lee YJ, Jung SE. Dynamic contrast-enhanced MRI of the prostate: can auto-generated wash-in color map be useful in detecting focal lesion enhancement? Investig Magn Reson Imaging 2019;23:220-227
5. Choi MH, Jung SE, Park YH, Lee JY, Choi YJ. Multiparametric MRI of prostate cancer after biopsy: little impact of hemorrhage on tumor staging. Investig Magn Reson Imaging 2017;21:139-147
6. Giannini V, Mazzetti S, Vignati A, et al. A fully automatic computer aided diagnosis system for peripheral zone prostate cancer detection using multi-parametric magnetic resonance imaging. Comput Med Imaging Graph 2015;46 Pt 2:219-226
7. Gao Y, Sandhu R, Fichtinger G, Tannenbaum AR. A coupled global registration and segmentation framework with application to magnetic resonance prostate imagery. IEEE Trans Med Imaging 2010;29:1781-1794
8. Ghose S, Oliver A, Marti R, et al. A survey of prostate segmentation methodologies in ultrasound, magnetic resonance and computed tomography images. Comput Methods Programs Biomed 2012;108:262-287
9. Tian Z, Liu L, Zhang Z, Fei B. Superpixel-based segmentation for 3D prostate MR images. IEEE Trans Med Imaging 2016;35:791-801
10. Klein S, van der Heide UA, Lips IM, van Vulpen M, Staring M, Pluim JP. Automatic segmentation of the prostate in 3D MR images by atlas matching using localized mutual information. Med Phys 2008;35:1407-1417
11. Chandra SS, Dowling JA, Greer PB, et al. Fast automated segmentation of multiple objects via spatially weighted shape learning. Phys Med Biol 2016;61:8070-8084
12. Greenham S, Dean J, Fu CK, et al. Evaluation of atlas-based auto-segmentation software in prostate cancer patients. J Med Radiat Sci 2014;61:151-158
13. Litjens G, Toth R, van de Ven W, et al. Evaluation of prostate segmentation algorithms for MRI: the PROMISE12 challenge. Med Image Anal 2014;18:359-373
14. Wang H, Suh JW, Das SR, Pluta JB, Craige C, Yushkevich PA. Multi-atlas segmentation with joint label fusion. IEEE Trans Pattern Anal Mach Intell 2013;35:611-623
15. Smith SM, Jenkinson M, Woolrich MW, et al. Advances in functional and structural MR image analysis and implementation as FSL. Neuroimage 2004;23 Suppl 1:S208-219